physica status solidi a
www.pss-a.com
applications and materials science

Raman spectroscopy of WO_3 nano-wires and thermo-chromism study of VO_2 belts produced by ultrasonic spray and laser pyrolysis techniques

B. W. Mwakikunga[1, 2, 3], E. Sideras-Haddad[2], A. Forbes[4, 5], and C. Arendse[1]

[1] CSIR National Centre for Nano-Structured Materials, P.O. Box 395, Pretoria 0001, South Africa
[2] School of Physics, University of the Witwatersrand, Private Bag X3, P.O. Wits, Johanneburg 2050, South Africa
[3] Department of Physics and Biochemical Sciences, University of Malawi, The Polytechnic, Private Bag 303, Chichiri, Blantyre 3, Malawi
[4] CSIR National Laser Centre, P.O. Box 395, Pretoria 0001, South Africa
[5] School of Physics, University of Kwazulu-Natal, Private Bag X54001, Durban 4000, South Africa

Received 2 May 2007, accepted 25 October 2007
Published online 15 January 2008

PACS 63.22.+m, 73.63.Bd, 78.30.Hv, 81.07.Bc, 81.15.Rs, 81.16.Mk

Novel optical and electrical properties of newly synthesized nano-wires of monoclinic WO_3 and nano-belts of rutile VO_2 have been investigated by Raman spectroscopy and thermo-chromism studies respectively. Phonon confinement is observed in the WO_3 nano-wires and the previously modified Richter equation is fitted to the experimental Raman spectroscopy data to obtain the optical phonon dispersion relations for the 713 cm^{-1} branch and the 808 cm^{-1} branch of WO_3 phonon spectra for the first time. Electrical measurements on the VO_2 nano-belts at varying temperature reveal an enhanced hysteresis width of about 83 °C surpassing previously reported values on the thermo-chromism studies on VO_2.

phys. stat. sol. (a) **205**, No. 1, 150–154 (2008) / **DOI** 10.1002/pssa.200776829

phys. stat. sol. (a) **205**, No. 1, 150–154 (2008) / **DOI** 10.1002/pssa.200776829

physica status solidi a
www.pss-a.com
applications and materials science

Raman spectroscopy of WO_3 nano-wires and thermo-chromism study of VO_2 belts produced by ultrasonic spray and laser pyrolysis techniques

B. W. Mwakikunga[1, 2, 3], E. Sideras-Haddad[*, 2], A. Forbes[4, 5], and C. Arendse[1]

[1] CSIR National Centre for Nano-Structured Materials, P.O. Box 395, Pretoria 0001, South Africa
[2] School of Physics, University of the Witwatersrand, Private Bag X3, P.O. Wits, Johanneburg 2050, South Africa
[3] Department of Physics and Biochemical Sciences, University of Malawi, The Polytechnic, Private Bag 303, Chichiri, Blantyre 3, Malawi
[4] CSIR National Laser Centre, P.O. Box 395, Pretoria 0001, South Africa
[5] School of Physics, University of Kwazulu-Natal, Private Bag X54001, Durban 4000, South Africa

Received 2 May 2007, accepted 25 October 2007
Published online 15 January 2008

PACS 63.22.+m, 73.63.Bd, 78.30.Hv, 81.07.Bc, 81.15.Rs, 81.16.Mk

[*] Corresponding author: e-mail elias.sideras-haddad@wits.ac.za, Fax: 0027 11 717 6879

Novel optical and electrical properties of newly synthesized nano-wires of monoclinic WO_3 and nano-belts of rutile VO_2 have been investigated by Raman spectroscopy and thermo-chromism studies respectively. Phonon confinement is observed in the WO_3 nano-wires and the previously modified Richter equation is fitted to the experimental Raman spectroscopy data to obtain the optical phonon dispersion relations for the 713 cm^{-1} branch and the 808 cm^{-1} branch of WO_3 phonon spectra for the first time. Electrical measurements on the VO_2 nano-belts at varying temperature reveal an enhanced hysteresis width of about 83 °C surpassing previously reported values on the thermo-chromism studies on VO_2.

1 Introduction Single crystalline semiconductor nano-wires are being extensively investigated due to their unique electronic and optical properties and their novel use in electronic and photonic devices. These unique properties arise from their anisotropic geometry, large surface-to-volume ratio, and carrier and photon/phonon confinement in two dimensions (1D system). More focus, in terms of electronic and photonic applications, is currently directed towards controlled synthesis and characterization of nano-wires (NWs) rather than nano-tubes (NTs) due to inability to control the electronic properties of NTs during synthesis. By contrast, the ability to rationally fabricate NWs with precisely controlled and tuneable chemical composition, size, structure and morphology and to accurately dope them with both p- and n-type dopants has opened up opportunities for assembling almost any kind of functional nano-system ranging from integrated solid-state photonics and electronics to biological sensors [1]. For example, NWs have been organized into field effect transistors, bipolar junction transistors, integrated logic calculators, high frequency ring oscillators and biological and chemical sensors, with some having detection limits down to a single virus [2]. Nano-photonic devices such as light-emitting diodes (LEDs), waveguides, electrically-driven single NW-based lasers, photo-detectors and avalanche photodiodes have all been successfully demonstrated [3].

WO_3 and VO_2 rutile (VO_2 (R)) are transition metal oxides (TMOs) whose properties are superior in their respective families of WO_x and VO_x (x is the O/metal ratio). At room temperature they both adopt distorted structures of some more symmetrical TMOs respectively ReO_3 and TiO_2 [4]. WO_3 has been used as an active layer with outstanding electro-chromic [5], gaso-chromic [6] and photo-chromic [7] properties. For this reason, WO_3 has been used to con-

struct flat panel displays, photo-electro-chromic 'smart' windows [8], writing-reading-erasing optical devices [9], optical modulation devices [10], gas sensors and humidity and temperature sensors [11]. On the other hand, VO_2 is thermo-chromic [12] and due to this structural change, depending on ambient temperature, VO_2 has a myriad of quite similar application to WO_3: energy efficient windows, optic disc media and holographic storage, bit recording, write-erase stable devices ultra fast switches and I.R. and radar camouflage and laser protection in the military [12].

For a perfect crystal of diameter d having vibrational modes of momentum $\boldsymbol{q}$, the Heisenberg's uncertainty principle ($\delta d\,\delta \boldsymbol{q} \sim h$) means that as $\delta d \to \infty$ (bulk) then $\delta \boldsymbol{q} \to 0$ (the $\boldsymbol{q} = 0$ selection rule applies). As the diameter, $\delta d \to 0$ (nano-metric) then the vibrational momentum, $\delta \boldsymbol{q} \to \infty$. In this case, a contribution from the $\boldsymbol{q} \neq 0$ phonons determined by the dispersion relation $\omega(\boldsymbol{q})$ is allowed. This accounts for the asymmetric broadening of the peaks in a Raman spectrum. The Richter equation for confined phonons in spherical nano-particles [15], modified to include Gaussian distribution of the phonon momenta and particle size by Faucet and Campbell [16], and further modified to account for the geometry of nano-wires by Adu et al. [11, 17] has been used herein to obtain phonon dispersion spectra for WO_3.

Thermo-chromism – the ability to change VO_2 (R)'s colour at different ambient temperatures – is one of this material's many important optical properties. This colour change displays a hysteresis around 68 °C. The hysteresis width (HW) determines the materials stability especially when used in optical data storage and optical/electrical switching applications. HW values in the range 1–10 °C have been reported by DeNatale et al. (1989) (in Ref. [14]). We have reported an HW of 5 °C in VO_2 (R) produced by ultrasonic spray pyrolysis [12]. A remarkably enhanced hysteresis was report by Lopez et al. [14] to the value of 34 °C on which we have made an improvement in the current study as discussed in the results section.

2 Experimental Two techniques were used in the synthesis of WO_3 and VO_2 (R) nanostructures: ultrasonic spray pyrolysis (USP) and laser pyrolysis (LP) [20, 21]. Synthesis of WO_3 and VO_2 by USP has been reported previously [12]. In brief, and as illustrated in Fig. 1(a), these processes involve decomposition of the relevant precursor droplets at atmospheric pressure in temperature regions of 100–700 °C and depositing the solid state particles that form on Corning glass substrates. The precursor droplets for USP were generated by focussing ultrasound waves of frequency, f, to the surface of the precursor liquid of surface tension, σ and density, ρ thereby producing droplets of typical diameter $D = k(\pi\sigma/\rho_{pr})^{1/3}$. The solid state particles so-obtained have typical diameters $d = D(c_{pr} \cdot M_p/\rho_p \cdot M_{pr})^{1/3}$ where c_{pr} is concentration of precursor, M_p and M_{pr} are molar masses of precursor and deposited particles respectively; and ρ_p being the density of the as-deposited particles. Synthesis by LP has also been reported elsewhere [12, 20, 21]. This is schematically illustrated in Fig. 1(b). Droplets from precursors of WCl_6 (Aldrich 99.99%) in ethanol, VCl_4 (Aldrich 99.99%) in ethanol and aqueous V_2O_5 pre-molten at 800 °C were injected in a 50 W CO_2 laser beam by a nebuliser (Microlife, model NEB50). The beam, tuned at a wavelength of 10.59 μm, was focussed to 2.4 mm to completely engulf the injected droplets. Particles from these processes were deposited onto Corning glass (SiO_2) substrates and these were further annealed in argon atmosphere at 500 °C for 17 hours.

Morphology studies were carried out using a LEO 1525 field emission scanning electron microscope (FESEM) operated at 3–20 kV. Raman spectroscopy was carried out using a Jobin–Yvon T64000 Raman spectrograph with a 514.5 nm line from an argon ion laser. The power of the laser at the sample for Raman spectroscopy of the post-annealed samples was small enough (0.384 mW) in order to minimise localised heating of the sample. The T64000 was operated in single spectrograph mode, with

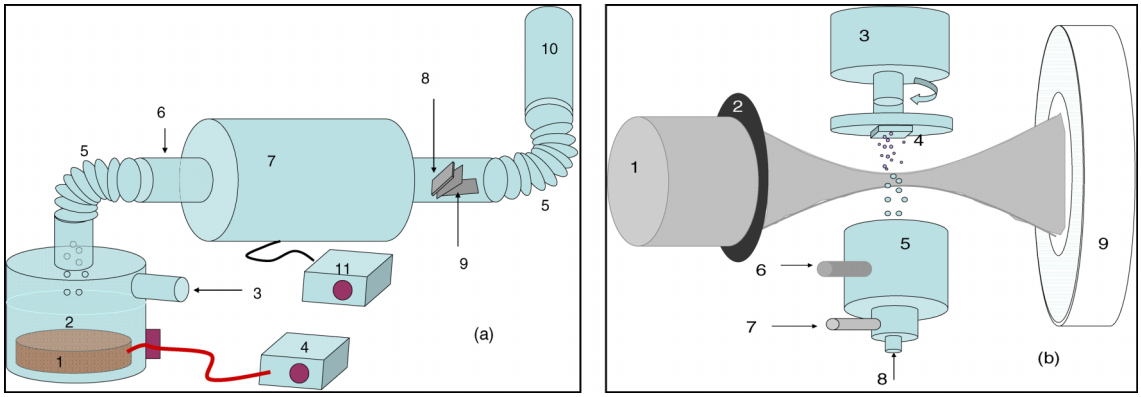

Figure 1 (online colour at: www.pss-a.com) (a) Schematic set up of ultrasonic spray pyrolysis: (1) ultrasonic nebuliser transducer, (2) precursor liquid, (3) carrier gas inlet, (4) nebuliser power supplier, (5) connecting bellow, (6) quartz tube, (7) tube furnace, (8) substrate, (9) substrate holder, (10) exhaust pipe, (11) furnace temperature controller. Figure 1(b) is the outline of the laser pyrolysis set up: (1) laser beam, (2) focussing lens, (3) stepper-motor, (4) substrate, (5) three-way nozzle, (6) argon gas inlet, (7) carrier gas inlet, (8) precursor liquid droplets and carrier gas inlet, (9) power meter.

the 1800 lines/mm grating and a 20× objective on the microscope. The Richter equation given in Refs. [17, 18] and herein reproduced as Eq. (1) was fitted to experimental data and the pertinent parameters were extracted:

$$I(\omega) = A_0 \int_{-\infty}^{\infty} \left[2\pi \boldsymbol{q}_\perp \frac{\exp\left(-\frac{\boldsymbol{q}_\perp^2 d^2}{2\alpha}\right)}{(\omega - \omega(\boldsymbol{q}))^2 + \Gamma_0^2/4} \right] \mathrm{d}\boldsymbol{q}_\perp \,. \qquad (1)$$

In the equation, d is the nano-wire diameter, α is the scaling factor, Γ_0 is the full-width-at-half-maximum (FWHM) for bulk material Raman peak ($\Gamma_0 = 6.5$ cm^{-1} for WO_3) [18], $\boldsymbol{q}_\perp$ signifies the momentum vectors perpendicular to the wire length, $\omega(\boldsymbol{q})$ is the phonon dispersion curve relation (PDR) for the material, $A = 713$ cm^{-1}, $a = 0.76$ nm for the 713 cm^{-1} phonon branch whereas $A = 808$ cm^{-1} and $b = 0.38$ nm [22–25] for the 808 cm^{-1} phonon branch. For the purposes of the fitting session, the phonon dispersion relation, $\omega^2(\boldsymbol{q}) = A^2 + AB \sin^2(a\boldsymbol{q}) + B^2 \sin^4(a\boldsymbol{q})$, was derived from the simple relation of the form $\omega(\boldsymbol{q}) = A + Ba^2\boldsymbol{q}^2$. The latter assumes isotropic dispersion curves [26]; however the former provided a much smoother fit than the latter for the present WO_3 Raman spectroscopy data. B was determined after non-linear fitting of Eq. (1) to experimental Raman spectral data. This was carried out using Mathmatca™.

Electrical resistances of the VO_2 (R) nanobelts (NBs) were measured at different points on the sample using a digital multi-meter and heated base coupled with a temperature controller. The Varian Cary 500 spectrophotometer was used to obtain transmittance of the material in the UV–Vis and near IR ranges for optical transition studies in VO_2 nano-structure. All experimental procedures showed good reproducibility of results.

3 Results and discussion Typical SEM results of WO_3 and VO_2 (R) by USP and LP are shown in Fig. 2. LP WO_3 NWs have the most probable diameter of 51 nm (14–300 nm) and the LP the VO_2 (R) NBs have the most probable (width × length) of (3 μm × 15 μm). The thickness of these belts is observed to be in tens of nano-meters as unveiled by X-ray diffraction (not shown). Raman spectra for LP WO_3 NWs display remarkable asymmetrical broadening. The phonon frequencies affected are 260 cm^{-1} and 700 cm^{-1} respectively assigned to W^{4+} states and the O–W–O bending modes [19, 22–25]. Minor phonon confinement effects are observed on the major phonon of

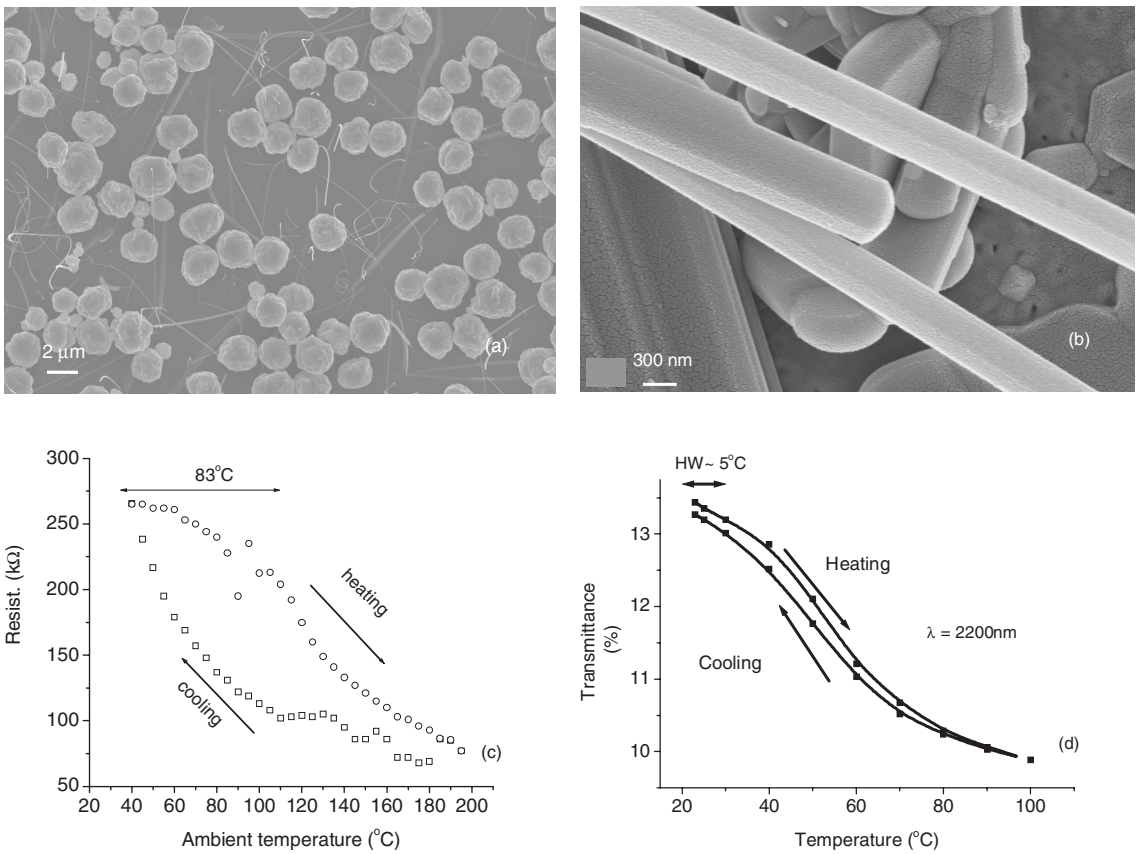

Figure 2 Characterization methods and results for WO_3 NWs and VO_2 NBs, (a) a typical SEM micrograph for WO_3 NWs and (b) SEM for VO_2 NBs; (c) VO_2 NBs enhanced electronic hysteresis plot compared to (d) the USP VO_2 optical transmittance hysteresis.

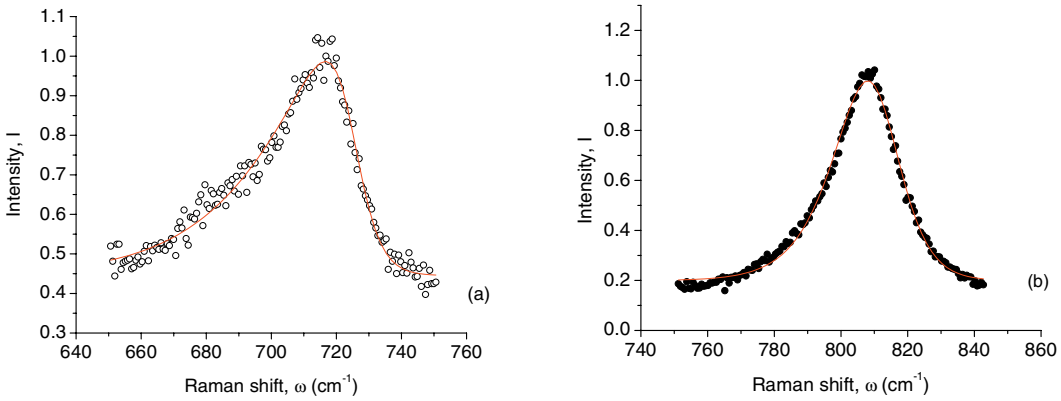

Figure 3 (online colour at: www.pss-a.com) Raman spectroscopy data plots for WO_3 NWs pertaining to the 713 cm^{-1} TO phonon (a) and the 808 cm^{-1} LO phonon (b) fitted with Eq. (1). The nano-wire diameter considered was 14 nm.

800 cm^{-1} assigned to O–W–O stretching mode and the 960 cm^{-1} assigned to $W^{6+}=O$ surface dangling bonds [18, 22–25]. Fitting of the Richter equation to the O–W–O bending mode Raman peak at 713 cm^{-1} (TO) yields a confinement scale factor of $\alpha = 7.0 \pm 3.0$, a pre-factor $A_0 = 9.9 \times 10^{-9}$ and a phonon dispersion parameter of $B = 0.14 \pm 0.05$ cm^{-2}. Similarly, for the LO phonon at 808 cm^{-1}, the scaling factor, $\alpha = 14 \pm 2$ and, $A_0 = 8.7 \times 10^{-13}$ and $B = 0.011 \pm 0.005$. The fitting sessions are summarised by an illustration in Fig. 2. By this technique, we have been able to obtain the phonon dispersion relations for the two phonon types (where $a = 0.76$ nm and $b = 0.38$ nm are lattice parameters [22]) for monoclinic WO_3 given as:

$$\begin{aligned} \omega_{\mathrm{TO}}^2(\boldsymbol{q}) &= 713^2 + 101 \sin^2 (a \cdot \boldsymbol{q}) + 0.0196 \sin^4 (a \cdot \boldsymbol{q}) \\ \omega_{\mathrm{LO}}^2(\boldsymbol{q}) &= 808^2 + 8.1 \sin^2 (b \cdot \boldsymbol{q}) + 0.0001 \sin^4 (b \cdot \boldsymbol{q}) \end{aligned} \quad . \quad (2)$$

Neutron scattering measurements on single crystals of $M_{0.33}WO_3$, a traditional experimental method for the determination of phonon dispersion curves, revealed low frequency, relatively dispersion-less phonon branches [26] but in the present study photon scattering shows considerable dispersion in stoichiometric WO_3. Different materials and different phonon types show differing values of the scale factor, α: For example, $\alpha = 6.3$ for Si NWs [18], $\alpha = 4$ for Si nano-particles [15], a contradictory $\alpha = 16\pi^2$ for Si NWs [31], $\alpha = 8\pi^2$ for (CdSe nano-crystals [28], c-BN nano-crystals [16], ZnO_2 nano-crystals [29]) where phonons are considered to be heavily confined and $\alpha = 30$ for anatase TiO_2 [30].

X-ray diffraction results (not shown here) show that the USP materials are a mixture of amorphous and polycrystalline particles whereas for LP high quality single crystals [(100) for LP WO_3 NWs)] and bi-crystalline [(110) and (210) peaks in LP VO_2NBs] are obtained. The broadening in a strong WO_3 NW X-ray diffraction peak centred at $2\theta = 26.81 \pm 0.02$ with an FWHM of 0.88 ± 0.10 was used to calculate the crystallite size. By employing the Debye–Scherrer equation assuming a standard width of 0.33° for bulk WO_3, the calculation yielded a crystallite size of 4.6 nm. The metal-to-semiconductor and optical and electronic transitions in VO_2 (R) are given in Fig. 1(c) and (d) and these display enhanced hysteresis especially in VO_2 (R) NBs synthesized by LP with a hysteresis width of >83 °C which is much higher than the highest previously reported value according to Lopez et al. [14] of only about 34 °C. Our HW value by USP was equally low (~5 °C) [see Fig. 1(d)]. This anomalous behaviour could be due to resilience to structural-transformation in ultra-thin VO_2 belts (as confirmed by the broadened X-ray diffraction peaks (not shown)). However, the shift to higher temperature is attributed to carbon impregnation when running the synthesis under acetylene gas. It has been found in numerous previous studies that doping VO_2 with ions of lower valence than 4+ increases its transition temperature whereas doping with ions of greater valence than 4+ does the reverse. Since the valences for carbon and vanadium are comparable in this case, we can conclude that comparable valence increases the VO_2 transition temperature; this fact has to be investigated further using other types of elements of valence of 4+.

4 Conclusion We have synthesized WO_3 and VO_2 (R) nanostructures by two related methods: USP and LP. Micro-sized and nano-sized particles were obtained by USP; however, WO_3 NWs and VO_2 (R) NBs were obtained by LP. Phonon confinement is observed especially in those materials synthesized by LP and phonon dispersion relations for WO_3 (given in Eq. (2)) were obtained for the first time by fitting the Richter equation for confined phonons to experimental data. Thermo-chromic characterization of VO_2 (R) NBs revealed an enhanced hysteresis width (HW ~ 83 °C) surpassing the highest reported value so far. This study shows the highly promising potential of LP as a materials processing technique in terms of improving the optical, photonic and electrical/electronic properties of materials.

Acknowledgements Financial and/or infrastructural sponsorship from C.S.I.R., National Research Foundation of South Africa and the African Laser Centre are acknowledged. The assistance of Retha Rossouw of NMISA and Henk van Wyk of CSIR-National Laser Centre is also acknowledged.

References

[1] R. Agarwal and C. M. Lieber, Appl. Phys. A **85**, 209 (2006).
[2] A. M. Morales and C. M. Lieber, Science **279**, 208 (1998).
[3] X. Duan, Y. Huang, R. Agarwal, and C. M. Lieber, Nature **421**, 241 (2003).
[4] P. A. Cox, Transition Metal Oxides: An Introduction To Their Electronic Structure and Properties (Oxford University Press, 1992), p. 20.
[5] C. G. Granqvist et al., Solar Energy **63**, 199 (1998).
[6] A. Hoel, L. F. Reyes, P. Heszler, V. Lantto, and C. G. Granqvist, Curr. Appl. Phys. **4**, 547 (2004).
[7] M. Bendahan, R. Boulmani, J. L. Seguin, and K. Aguir, Sens. Actuators **100**, 320 (2004).
[8] C. Bittencourt, R. Landers, E. Llobet, G. Molas, X. Correig, M. A. P. Silva, J. E. Sueiras, and J. Calderer, Electrochem. Soc. **149**, H81 (2002).
[9] M. Gillet, K. Aguir, M. Bendahan, and P. Mennini, Thin Solid Films **484**, 358 (2005).
[10] S. W. Wang, T. C. Chou, and C. C. Liu, Sens. Actuators B **94**, 343 (2003).
[11] V. Guidi et al., Sens. Actuators B **100**, 277 (2004).
[12] B. W. Mwakikunga, E. Sideras-Haddad, and M. Maaza, Opt. Mater. **29**, 481 (2007).
[13] B. W. Mwakikunga, A. Forbes, E. Sideras-Haddad, R. Erasmus, G. Katumba, and B. Masina, Int. J. Laser Nanomanuf. (2007) (accepted).
[14] R. Lopez, L. A. Boatner, T. E. Haynes, L. C. Feldman, and R. Hugland, J. Appl. Phys. **92**, 4031 (2002).
[15] H. Richter, Z. P. Wang, and L. Ley, Solid State Commun. **39**, 625 (1981).
[16] P. M. Faucet and I. H. Campbell, Solid State Commun. **58**, 739 (1986); Crit. Rev. Solid State Mater. Sci. **14**, 79 (1988).
[17] K. W. Adu, H. R. Gutierrez, U. J. Kim, G. U. Sumanasekera, and P. C. Eklund, Nano Lett. **5**, 400 (2005).
[18] K. W. Adu, H. R. Gutierrez, and P. C. Eklund, Vib. Spectrosc. **42**, 165 (2006).
[19] M. Boulova, N. Rosman, P. Bouvier, and G. Lucazeau, J. Phys.: Condens. Matter **14**, 5849 (2002).
[20] J. S. Hagerty, in: Laser-Induced Chemical Process, edited by J. I. Steinfield (Plenum, New York, 1981).
[21] P. C. Eklund, X. X. Bi, and F. J. Derbyshire, Am. Chem. Soc., Fuel Chemistry Division **37**, 1781 (1992).
[22] E. Salje, Acta Cryst. B **33**, 574 (1977).
[23] S. H. Lee, H. M. Cheong, C. E. Tracy, A. Mascarenhas, D. K. Benson, and S. K. Deb, Electrochim. Acta **44**, 3111 (1999).
[24] Y. S. Huang, Y. Z. Zhang, X. T. Zeng, and X. F. Hu, Appl. Surf. Sci. **202**, 104 (2002).
[25] J. Grabrusenoks et al., J. Electrochim. Acta **46**, 2229 (2001).
[26] W. A. Kamitakahara, K. Scharnberg, and M. Shanks, Phys. Rev. Lett. **43**, 1607 (1979).
[27] A. K. Arora, M. Rajalakshmi, T. R. Ravindran, and V. Sivasubramanian, J. Raman Spectrosc. **38**, 604 (2007).
[28] A. Tanaka, S. Onari, and T. Arai, Phys. Rev. B **45**, 6587 (1992).
[29] T. Werninghaus, J. Hahn, F. Richter, and D. R. T. Zahn, Appl. Phys. Lett. **70**, 958 (1997).
[30] K. R. Zhu, M. S. Zhan, Q. Chen, and Z. Yin, Phys. Lett. A **340**, 220 (2005).
[31] S. Piscanec, M. Cantoro, A. C. Ferrari, J. A. Zapien, Y. Lifshitz, S. T. Lee, S. Hoffmann, and J. Robertson, Phys. Rev. B **68**, 241312 (R) (2003).

